Advanced Fiber Materials (2024) 6:1629–1639
https://doi.org/10.1007/s42765-024-00445-1

RESEARCH ARTICLE

Robust Fiber Strain Sensor by Designing Coaxial Coiling Structure with Mutual Inductance Effect

Yulu Ai[1,2] · Zhen Wang[1,4] · Yue Liu[1,2] · Yuanyuan Zheng[1,2,3] · Jiaqi Wu[1,2] · Junyi Zou[1,2] · Songlin Zhang[1] · Peining Chen[1,2,3] · Huisheng Peng[1,2,3,4]

Received: 13 March 2024 / Accepted: 26 May 2024 / Published online: 5 June 2024
© Donghua University, Shanghai, China 2024

Abstract

Fiber strain sensors with robust sensing performance are indispensable for human–machine interactions in the electronic textiles. However, current fiber strain sensors are confronted with the challenges of unavoidable deterioration of functional sensing components during wearable and extreme environments, resulting in unsatisfactory stability and durability. Here, we present a robust fiber strain sensor based on the mutual inductance effect. The sensor is assembled by designing coaxial helical coils around an elastic polyurethane fiber. When stretching the fiber sensor, the strain is detected by recording the voltage changes in the helical coils due to the variation in magnetic flux. The resultant fiber strain sensor shows high linearity (with a linear regression coefficient of 0.99) at a large strain of 100%, and can withstand various extreme environmental conditions, such as high/low temperatures (from − 30 °C to 160 °C), and severe deformations, such as twisting and pressing (with a pressure of 500 N/cm). The long-term cyclic stability of our fiber strain sensor (100,000 cycles at a strain of 100%) is superior to that of most reported flexible resistive and capacitive strain sensors. Finally, the mass-produced fiber strain sensors are woven into a smart textile system to accurately capture gestures.

Keywords Electronic textile · Fiber strain sensor · Mutual inductance effect · Coaxial coiling structure

1 Introduction

Smart textiles with diverse functionalities are indispensable for next-generation wearable electronics [1–4] in batteries [5–7], solar cells [8–10], displays [11, 12], and sensors [13–15]. Among these wearable electronics, smart textiles with sensing capabilities have attracted considerable interest in both academia and industry and have been deployed in daily scenarios for monitoring to purposes to achieve smart personal health care [16–18] and human–computer interactions [19–23]. Although patching traditional rigid sensing components onto textile substrates could enable sensing functions, these electronic textiles are confronted with the challenges of unstable performance, modulus mismatch, and wear discomfort. Fiber strain sensors can be directly woven or knitted into textiles, which has become an ideal approach for smart textile systems [24, 25]. However, the existing fiber strain sensors cannot meet the stability and durability requirements for daily use in worn or extreme environments such as fire rescue and space exploration.

Several common types of sensing mechanisms for fabricating fiber strain sensors, including resistive, capacitive, piezoelectric, and triboelectric mechanisms, have attracted extensive research interest [25, 26]. Although high strain sensitivity values have been reported in previous studies [24, 27–29], these sensors presented unsatisfactory stability and durability during wearable usage, including mechanical deterioration by compression, torsion, rubbing, machine washing, and low or high thermal damage. The functional materials (e.g., the sensing components) in these sensors are directly involved in device deformation when stretching or

Yulu Ai and Zhen Wang have contributed equally to the work.

✉ Peining Chen
peiningc@fudan.edu.cn

1 State Key Laboratory of Molecular Engineering of Polymers, Fudan University, Shanghai 200438, China

2 Department of Macromolecular Science, Fudan University, Shanghai 200438, China

3 Institute of Fiber Materials and Devices, Fudan University, Shanghai 200438, China

4 Laboratory of Advanced Materials, Fudan University, Shanghai 200438, China

compressing, resulting in unavoidable damage to the sensing materials. Consequently, the sensing data shift or drift after long-term cyclic operation. For instance, resistive strain sensors may suffer damage to threshold conductive pathways after cyclic stretching or compression at large strains [30–32]. Triboelectric strain sensors may suffer from triboelectric charge decay during the cyclic contact-separation process [33, 34]. Therefore, it is still challenging for fiber strain sensors to achieve robust sensing performance for long-term wear and extreme working conditions.

Herein, we report a robust fiber strain sensor based on the mutual inductance effect. Briefly, a pair of coaxial helical coils is wrapped around an elastic polyurethane (PU) fiber. The outer coils were aligned with the inner coils, and a polyurethane layer was placed between them for insulation. When stretching the fiber sensor, the pitch of the inner coils increases. Concomitantly, the reduction in magnetic flux variation in the outer coils was recorded and represented as a voltage drop. Benefiting from the unique sensing mechanism and structural design, such fiber strain sensors demonstrate superior stability and durability after long-term cyclic operation at large strains. Concisely, the fiber strain sensor exhibits excellent sensing response linearity (with a linear regression coefficient of 0.99) in a wide strain range (0–100%), superior sensing stability (100,000 cycles at 100% strain), and satisfactory reliability and durability (highly resistant to high/low temperature and severe deformations). We also showcase the potential of our fiber strain sensor for wearable applications by weaving it into a textile glove that successfully and accurately recognizes different hand gestures.

2 Experimental Section

2.1 Materials

N,*N*-dimethylformamide (DMF), $BaTiO_3$, polyurethane, polyurethane fiber and copper wire were purchased from Adamas. Waterborne polyurethane was purchased from Shanghai Sisheng Polymer Materials Company. Silver-plated nylon yarns (100D) were purchased from Suzhou Teck Silver Fiber Technology Company. Fluorine rubber (FR) was purchased from Daikin Fluorochemicals Company. The dispersion of silver nanowires was purchased from Jiangsu Xianfeng Nanomaterials Technology. A commercial capacitive sensor was purchased from TE Connectivity. These materials were used as received without further treatment.

2.2 Fabrication of the Fiber Strain Sensor

The fabrication process mainly includes four steps: (1) winding of the inner helical coils, (2) coating of the polyurethane encapsulation layer, (3) drying, and (4) winding of the outer helical coils. Specifically, PU fibers and copper wires (with a diameter of 50 μm) were separately passed through customized circular openings on a rotating disc. The copper wire was uniformly wound around the PU fiber when the disc rotated. The pitch of the inner coils was controlled by the rotational speed and the feed rate of the wire on the winding equipment (equation S1). The fiber was then immersed in a polyurethane solution (with a concentration of 5 wt%) and dried in an oven (at 60 °C) for 1 h to remove *N*,*N*-dimethylformamide. Finally, a fiber strain sensor with a coaxial coiling structure was obtained after winding an additional insulated copper wire (with a diameter of 50 μm) onto the as-prepared fiber.

2.3 Fabrication of the Smart Sensing Textile and Electronic Glove

Before weaving, a protective layer was incorporated onto the fiber to mitigate wear on the polyurethane coating during utilization (Fig. S1). PU fibers wound with inner helical coils were used as warp threads, and an outer copper wire wound around the warp served as the weft thread. The weaving process was conducted by using a rapier loom. By adjusting the position of the outer helical coils, fiber strain sensors are woven into specially-made elastic gloves to form a sensing array.

2.4 Fabrication of Luminous Yarns and Displaying Textile

$BaTiO_3$ particles were dispersed in a 12 wt% FR/DMF solution with a weight ratio of 3:1 and coated onto silver-plated nylon yarns, followed by solvent removal at 180 °C. Similarly, a mixture of ZnS phosphor and waterborne polyurethane with the same weight ratio was coated onto the yarns. The dispersion of silver nanowires was then dip-coated onto the yarns, which were wound with copper wires to increase electrical conductivity. A polyurethane layer was dip-coated onto the luminescent yarns to ensure water resistance. Through the rope embroidery process, luminous yarns were woven into the garment to obtain displaying textile.

2.5 Characterization

The sensing performance and stability of the fiber strain sensor were tested with a motion controller (TC55, TOPCNC, China), a signal generator (Model 645, Berkeley Nucleonics Corp., USA), an electronic universal tensile testing machine (HY-0305, Shanghai Hengyi Corp., China) and an oscilloscope (DSOX1202G, Keysight Technologies, USA). The above equipment was used for cyclic and dynamic force tests on a mechanized X-axis loading

platform. The controller was responsible for controlling the speed, distance, and cycles of movement. Real-time and dynamic output voltage signals were recorded using an oscilloscope (DSOX1202G, Keysight Technologies, USA). The smartphone could display real-time output voltage signals by connecting wireless Wi-Fi modules with sensing textiles.

3 Results and Discussion

3.1 Preparation and Characterization

Figure 1a shows the structure of fiber strain sensors that can be woven into textiles. Each fiber strain sensor consists of a PU fiber wound with inner and outer helical coils made of fine copper wire, where the inner helical coils serve as the electrical signal input, while the outer coils serve as the electrical signal output. A PU layer for insulation encapsulation was coated between the coils to prevent short circuits. As the fiber is stretched, the increase in the pitch of the inner/outer helical coils causes a decrease in the magnetic flux variation in the outer coils based on the principle of mutual inductance. Then a voltage change is generated to display the strain variation.

In a typical fabrication process, the coaxial coiling structure of the fiber strain sensor was fabricated through a coaxial winding method (Fig. 1b). Commercial PU fibers with diameters ranging from 300 μm to 900 μm were selected as the substrate. Specifically, the PU fiber and copper wire (with a diameter of 50 μm) were separately passed through two circular openings on a customized rotating disc. When the disc rotated, the copper wire was uniformly wound around the PU fiber with a certain pitch. The pitch of the inner helical coils was precisely controlled by varying the rotation speed of the circular disk and the feeding speed of the PU fibers (equation S1). As demonstrated in Fig. 1c and Fig. S2, the PU fiber could be wound with inner helical coils with pitches ranging from 100 μm (helical angle of 86°) to 600 μm (helical angle of 56°). The as-prepared fiber was then encapsulated by coating with a polyurethane solution at a concentration of 5 wt%, followed by heating to remove the solvent. Subsequently, the outer helical coils were fabricated by the same twisting method. Figure 1d shows the coaxial coiling structure of the fiber strain sensor. Fibers wound with helical coils maintain good flexibility, ensuring the accurate functioning of fiber strain sensors (Fig. 1e). The narrow pitch distribution of 100 counts in 100 m indicated the high reproducibility of the fabrication method (Fig. 1f). Using customized industrial equipment, we can mass-produce spools of flexible fibers with helical coils (Fig. 1g).

3.2 Sensing Performance

The performance of the fiber strain sensor was investigated as displayed in Fig. 2a, where the inner helical coils were applied with a constant alternating voltage while the outer coil was connected to a voltmeter. As the fiber is stretched, the decrease in the pitch of the inner and outer helical coils will reduce magnetic flux variation, a variation in the output voltage thus generated by the outer helical coils based on the mutual inductance effect.

The influences of the electrical and device structure parameters of the fiber strain sensor on the output voltage behaviors were first investigated. Fiber strain sensors require high-intensity signals to increase the signal-to-noise ratio. When an input alternating voltage with a peak-to-peak value ranging from 2 V to 10 V was applied to the inner coils, the outer coils generated an output voltage ranging from 0.7 V to 2.55 V (Fig. S3). With the input voltage maintained at 10 V, the change ratio of the output voltage was stably maintained at 19.7% with a slight fluctuation of 0.1% (at a strain of 100%), which is much smaller than the fluctuations observed at other input voltages (Fig. S3). This result also indicated that a higher output voltage could effectively mitigate signal interference. The frequency of the input alternating voltage also obviously affected the output voltage variation. The output voltage reached the maximum value (2.55 V) when the frequency of the input alternating voltage was 38 MHz, and the change ratio of the output voltage gradually decreased to 15% when the frequency was further increased to 46 MHz (Fig. S4). As the peak-to-peak value and frequency of the input alternating voltage were constant, the cross-sectional area and ratio of turns between the outer helical coils and the inner helical coils ($R_{o/i}$) were also crucial parameters for the sensing quality of the output voltage. For instance, the change ratio of the output voltage increased from 13% to 27% as the diameter of the fiber increased from 300 μm to 900 μm. A similar increase in the output voltage variation occurred when $R_{o/i}$ increased from 3:1 to 3:5 (Fig. S5). Furthermore, the fiber strain sensor generated a higher output voltage with a smaller helical pitch (Fig. S5), which could also effectively prevent signal interference during stretching. Unless otherwise stated, to ensure that the fiber strain sensor has a high signal-to-noise ratio, the diameter, and the pitch of the helical coils, and the $R_{o/i}$ in the following study were 600 μm, 50 μm, and 1:1, respectively; the peak-to-peak voltage and frequency of the input alternating voltage were 10 V and 38 MHz, respectively.

Systematic tests were carried out to showcase the sensing performance of the fiber strain sensor. The output voltage variation increased linearly (with a linear regression coefficient of 0.99) as the fiber strain sensor was stretched to 100% with a strain rate of 20% per second (Fig. 2b). The negligible discrepancies between the stretching/releasing

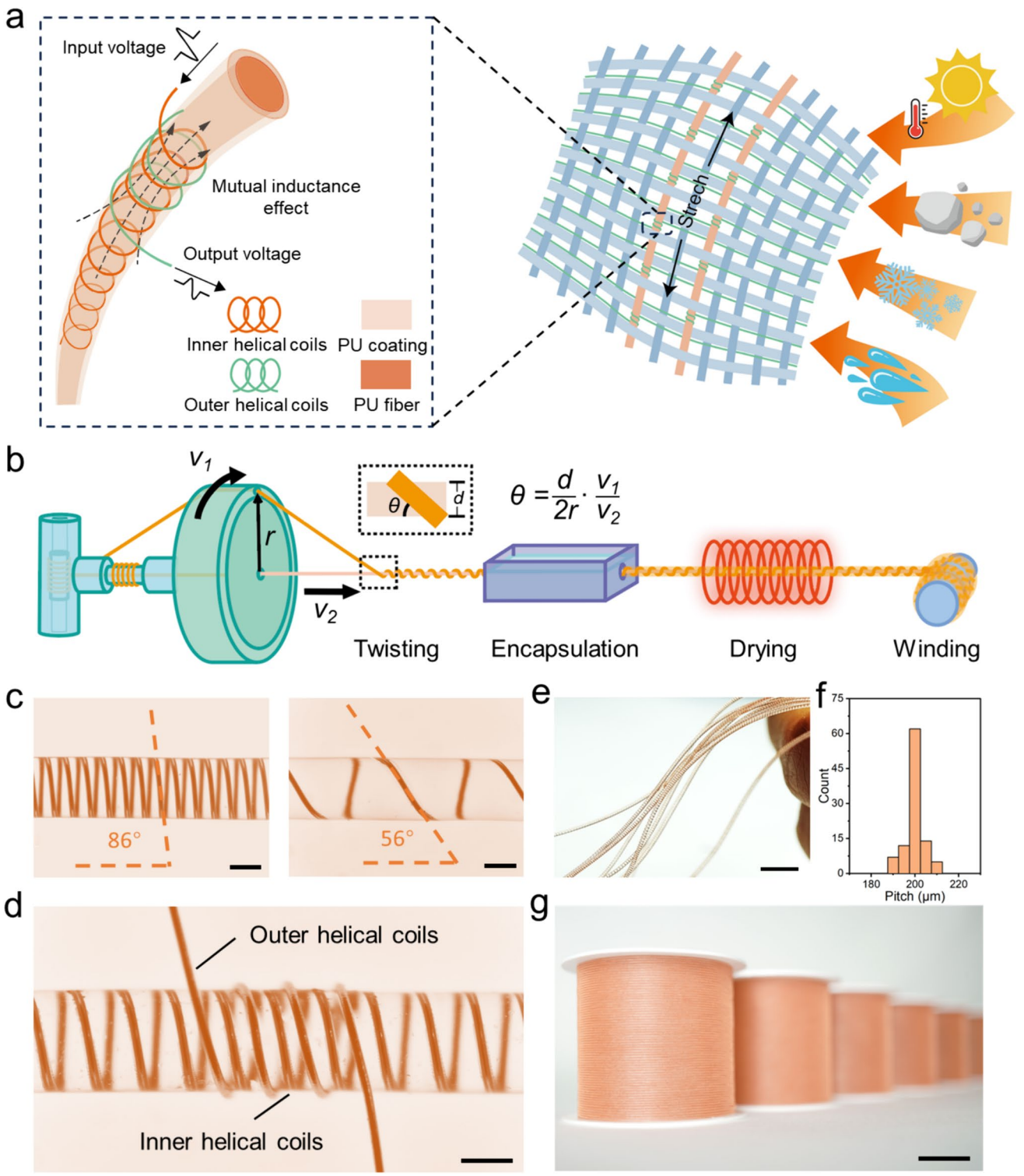

Fig. 1 Design and fabrication of the fiber strain sensor. **a** Schematic diagram showing the coaxial coiling structure of a fiber strain sensor woven in a textile. **b** Schematic diagram showing the fabrication process of the fiber strain sensor. **c** Photographs of fiber strain sensors with helical angles of 86° (left) and 56° (right); the corresponding pitches were 100 μm and 600 μm, respectively. **d** Microscope photo displaying the structure of the fiber strain sensor. **e** Photograph of the flexible fiber strain sensors. **f** The distribution of the pitches (amounting to 100 counts) of the fiber strain sensor with a length of 100 m. **g** Photograph of spools of fiber strain sensors. Scale bars: 300 μm (**c**), 300 μm (**d**), 5 mm (**e**), and 15 mm (**g**)

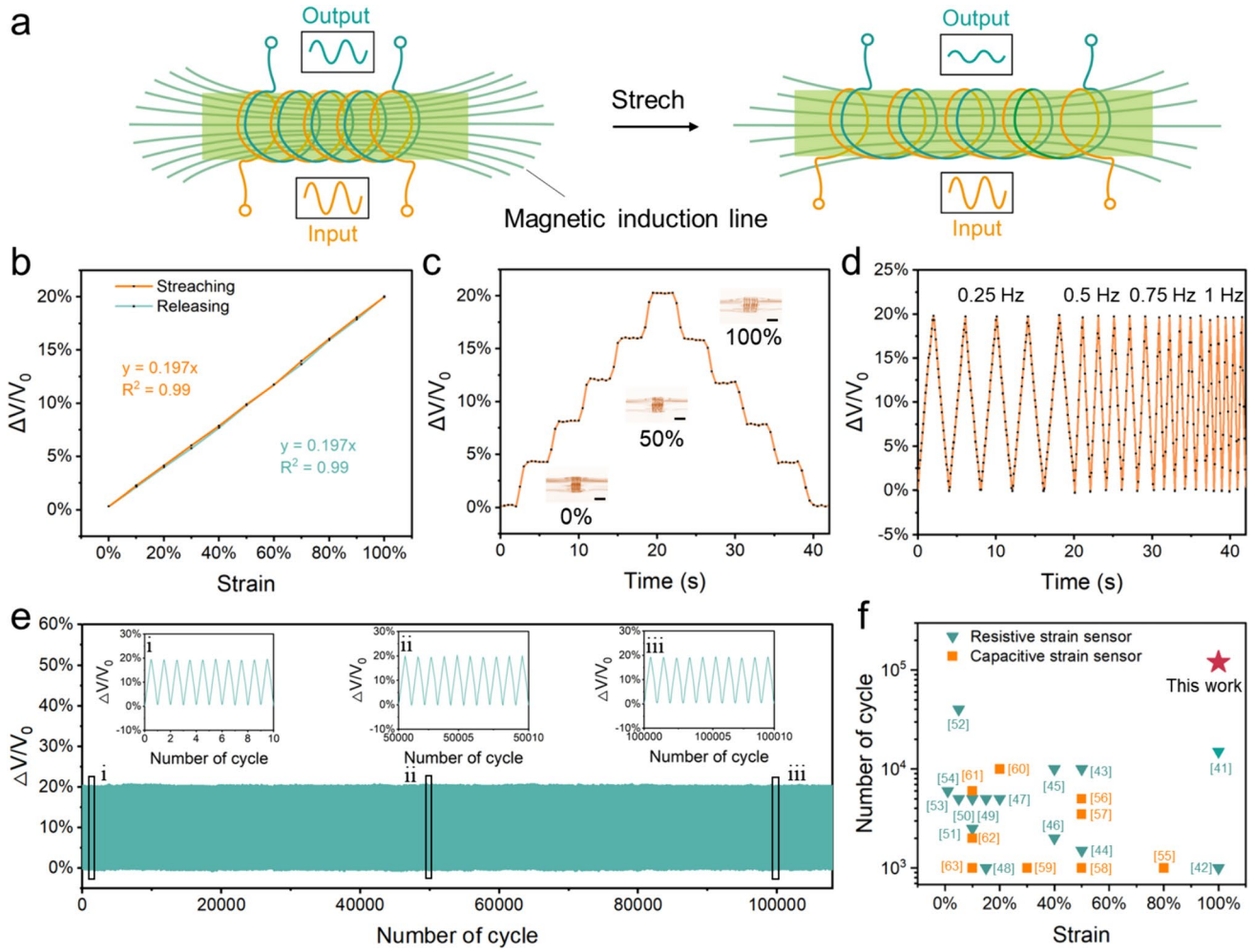

Fig. 2 Performance and stability of the fiber strain sensor. **a** Schematic diagram showing the working principle of the fiber strain sensor. **b** Variations in the output voltage when the fiber strain sensor is stretched to 100% strain at a strain rate of 20% per second. **c** Variations in the output voltage for fiber strain sensor under a series of strain step cycles from 20% to 100%. Insets: photographs of the sensor at 0%, 50%, and 100% strain; scale bars, 500 μm. **d** Dynamic stability of the fiber strain sensor in the frequency range of 0.25–1 Hz. **e** Variations in the output voltage for the fiber strain sensor over 100,000 stretching/releasing cycles at 100% strain, with close-up views at the beginning, middle and end of the test. **f** Comparisons of fiber strain sensors in this work with previously reported resistive [41–54] and capacitive [55–63] strain sensors in terms of the number of cycles and strain

curves indicated the low hysteresis of the fiber strain sensor. We evaluated the degree of hysteresis (*DH*) to assess this behavior via Eq. (1) [35, 36].

$$DH = \frac{A_{Loading} - A_{Unloading}}{A_{Loading}} \times 100\% \quad (1)$$

where $A_{Loading}$ and $A_{Unloading}$ represent the areas below the loading and unloading curves, respectively. A smaller *DH* value indicates a smaller hysteresis [37]. The fiber strain sensor showed a very small *DH* value of 1.3%, which is lower than that of most flexible resistive strain sensors [38, 39]. The sensitivity of the fiber strain sensor was evaluated by gauge factor (GF), which is defined as $(\Delta V/V_0)/(\Delta L/L)$. The sensitivity could be tuned from 0.11 to 0.68 by changing the frequency of input alternating voltage, diameter of fiber and *Ro*/*i*, which is comparable to typical strain sensors (Tables S1, S2). By measuring peak-to-peak voltage after applying a strain of 10%, the response time of the fiber strain sensor was 40 ms, which is superior to that of the most strain sensors (Fig. S6, Table S3). Figure 2c shows variations in the fiber strain sensor output voltage in a step-and-hold test where the sensor was subjected to alternating stepwise stretching with a 20% strain step size and holding (2.5 s). The applied strain increases to a maximum of 100% and then decreases to zero. The output voltage in each strain stage was nearly the same as that in each corresponding release stage, and no obvious "shoulder peaks" were observed under each strain, indicating the small overshoot behavior of the

fiber strain sensor [40]. Moreover, the fiber strain sensor exhibited good dynamic stability under large strain. The response characteristics under a stretching frequency of 1 Hz and strain of 100% were consistent with those under a stretching frequency of 0.25 Hz (Fig. 2d).

The stability of the fiber strain sensors was verified by performing a long-term cyclic tensile test, where the output voltage was continuously recorded under each stretching/releasing process (with a strain of 100%). As shown in Fig. 2e, the output voltage curve of the fiber strain sensor was nearly unchanged over the investigated 100,000 stretching/releasing cycles. An enlarged view of 10 cycles at the early, middle, and late stages of the cyclic tensile test demonstrated that the change ratio of the output voltage during both the stretching and releasing processes was stable (varied by less than 0.5%). This cyclic stability of over 100,000 cycles under a large strain of 100% based on the coaxial coiling structure of the fiber strain sensor is superior to that of reported flexible resistive [41–54] and capacitive [55–63] strain sensors, which typically withstand at most 10,000 stretching/releasing cycles under strains less than 50% (Fig. 2f).

3.3 Durability under Extreme Environments

For practical wearable applications, fiber strain sensors must endure various complex service conditions (Fig. 3a). To verify the durability of the fiber strain sensors, we performed various tests under different conditions, such as high/low temperatures, complex deformations and even water immersion/washing. The fiber strain sensor worked normally at a high temperature of 160 °C and a low temperature of − 30 °C, which applies to most areas on Earth. Because of the stable coaxial coiling structure of the fiber strain sensor, its performance remained unchanged even after vigorous complex deformations. For instance, when subjected to a torsional deformation of more than 1 080°, the fiber strain sensor showed slight output voltage fluctuations (less than 0.4% of the initial value). Moreover, the fiber strain sensor could withstand long-term water immersion because of the efficient polymer encapsulation. At a bending angle of 180°, the output voltage of the fiber strain sensor was only reduced by 0.06 V (2.4% of the initial value) due to the small size of the sensing unit (Fig. S7). Compression is another practical application environment that fiber strain sensors usually encounter. When a pressure of 500 N/cm was applied to the fiber strain sensor (Fig. 3b, c), the output voltage changed by 37.1% due to the decrease in the cross-sectional area (Fig. 3d). The fiber strain sensor could even work normally after repeated pressing processes. Moreover, the fiber strain sensor also showed good long-term cyclic stability under complex conditions. As shown in Fig. S8, the output voltage remained almost unchanged over 1000 cycles (with a strain of 100%) under high/low temperature. The change ratio of the output voltage was also stably maintained at 19.7% with a slight fluctuation of 0.6% after long-term washing, 10,000 bending, pressing and twisting cycles.

To further demonstrate the durability under extreme conditions, the fiber strain sensor was compared with typical resistive strain sensor based on AgNWs/PDMS-based [64] and commercial capacitive strain sensor (Fig. 3e). The resistive and capacitive sensors failed to return to their original state after torsion deformations (a 180°/5 cm twist applied 4 times) due to the irreversible damage of the AgNWs network for the resistive strain sensor and permanent deformation of the dielectric layer for the capacitive strain sensor (with offsets compared to the initial signal values of 1600% and 18%, respectively). Similarly, high-temperature conditions caused severe deformation of the polymer substrate in the resistive and capacitive strain sensors, thus resulting in performance degradation and functional failure. In comparison, under the same torsion or high-temperature conditions, the output voltage of the fiber strain sensor remained stable, with a small variation of less than 1%. This stability and durability may be attributed to the stable coaxial coiling structure and the sensing mechanism based on the mutual inductance effect. To validate the sensing robustness of the fiber strain sensor, we used the finite-element method to compare the stress distribution of the coaxial coiling structure in this study and bi-layered structure representing typical structure of resistive fiber strain sensors [24, 65, 66] (Fig. 3f, g and Table S4). At the same bending radius of 1 cm, the stress exhibited by the bi-layered structure was 3 times that of the coaxial coiling structure, indicating a small amount of stress between the coil and substrate in the fiber strain sensor.

3.4 Applications

Fiber strain sensors serving as warp threads could be woven into large-area sensing textiles by an industrial rapier loom (Fig. 4a–c), in which segmented outer helical coils could be wound around the fiber strain sensor at different positions to form a series of sensing units (Fig. 4c). As a proof-of-concept demonstration, we showed the wearing application potential of this sensing textile under extreme environments such as outer space (Fig. 4d). As shown in Fig. 4e, the output voltage was stable at 2.55 V even though the sensing textile was frozen in ice (at a low temperature of − 29 °C) for five days (Fig. 4f). When the sensing textiles were immersed in hot water at 95 °C (Fig. 4g) and subjected to a vacuum of 0.02 MPa (Fig. 4h), the output voltage curve remained stable without obvious fluctuations. Moreover, the sensing textile could even work normally after a car weighing 1720 kg rolled over it (Fig. 4i). By rationally arranging the sensing units in the sensing textile, a smart electronic glove was fabricated with sensing unit arrays to achieve real-time capture of gestures to control of the display

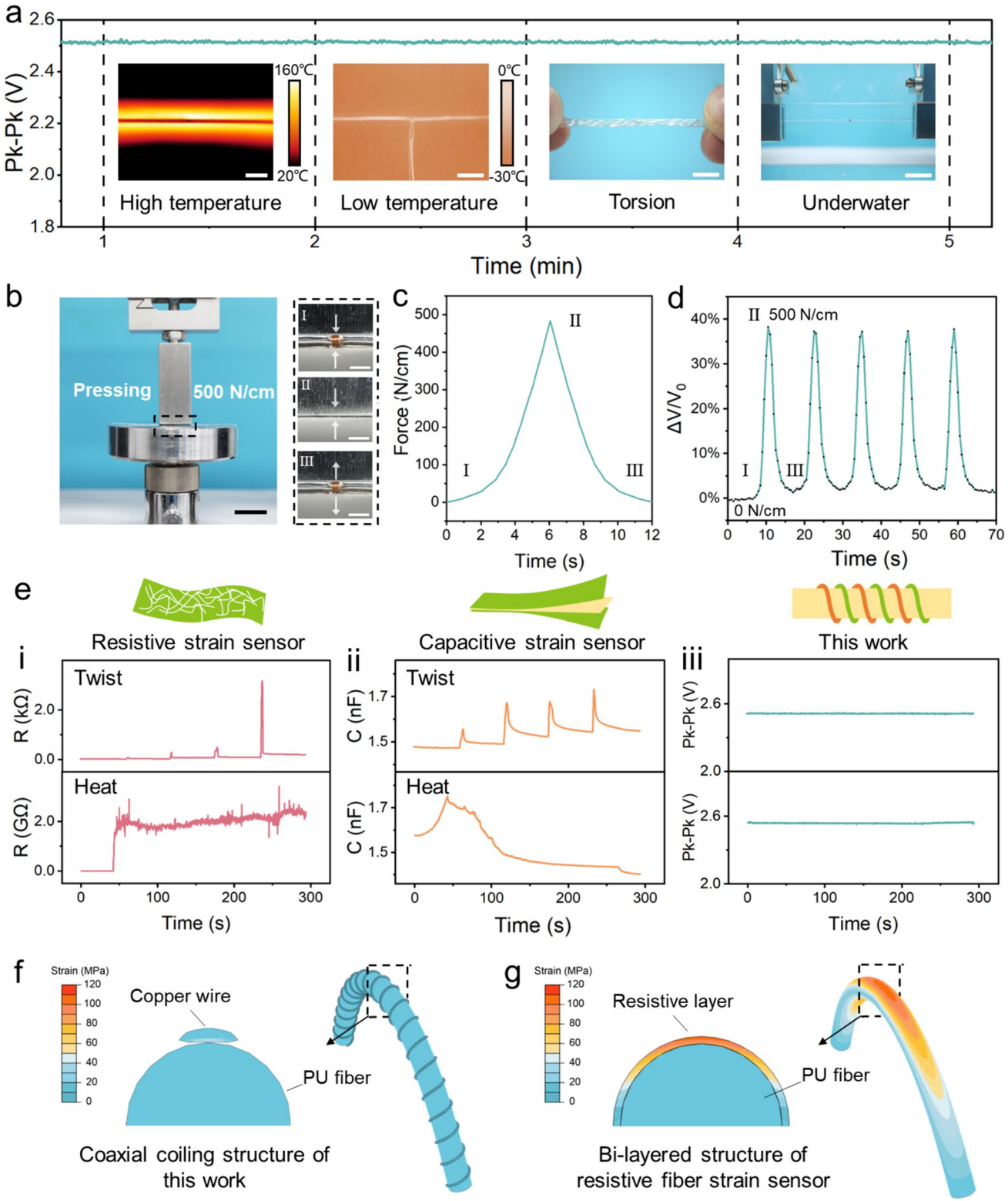

Fig. 3 Durability of the fiber strain sensor in extreme environments. **a** Output voltage of the fiber strain sensor under high/low temperature, torsion deformation and water immersion conditions; Pk–Pk: peak-to-peak voltage. **b** Photograph of the pressing test on the sensor. Insets: Photographs of squeezing and recovery process. **c** The tension induced by the tensile testing machine during the pressing and recovery process. **d** Variations in the output voltage over time during the pressing and recovery process. **e** Response of the resistive (i), capacitive sensors (ii), and this work (iii) under torsion (with a 180°/5 cm twist applied 4 times) and heating from 30 °C to 150 °C. **f**, **g** Finite element analysis of a fiber strain sensor with coaxial coiling and bi-layered structure. Scale bars: 1 cm (**a**), 2 cm (**b**), 800 μm (insets of **b**)

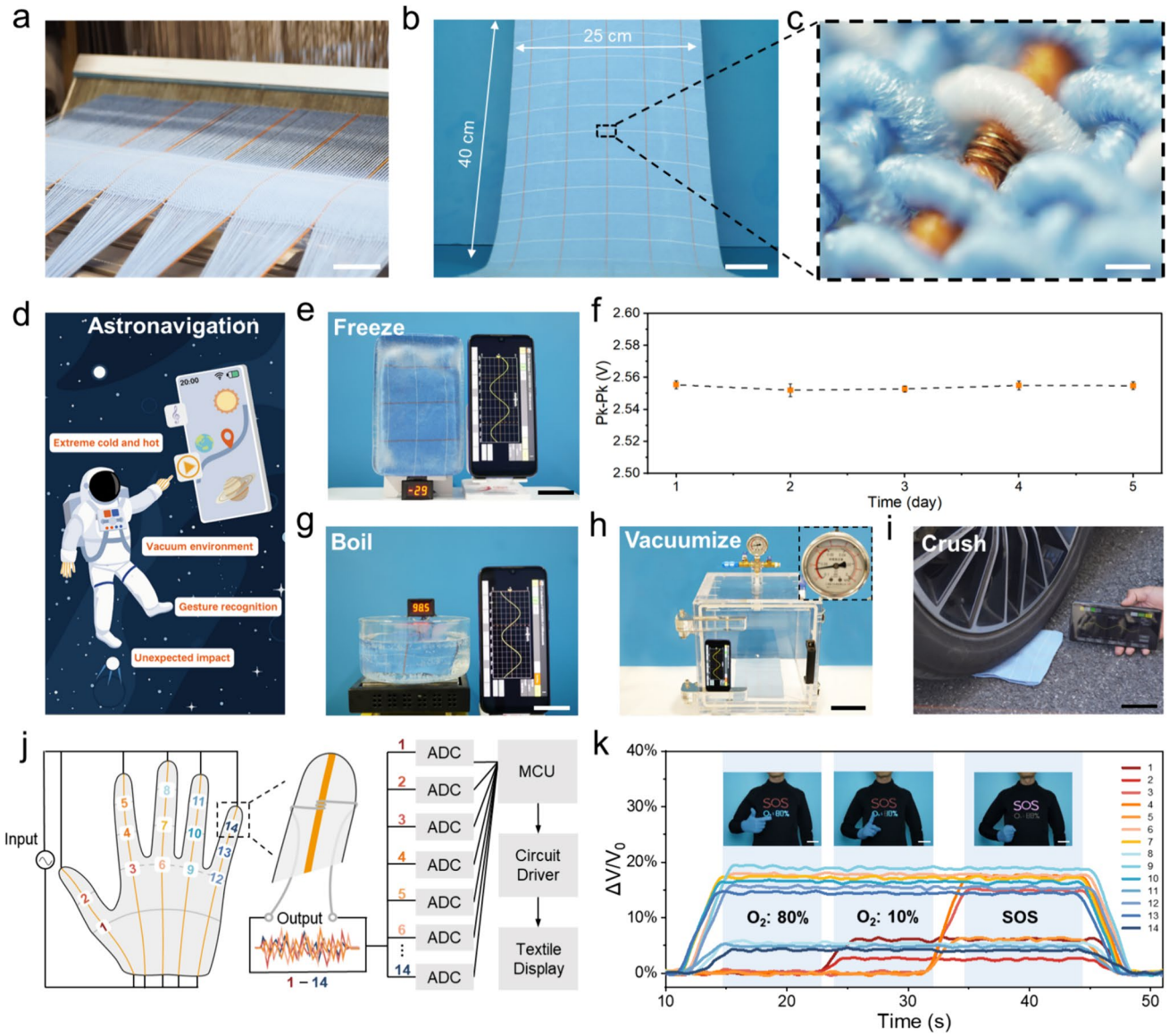

Fig. 4 Applications of the fiber strain sensor. **a** Photograph showing the fiber strain sensor woven into the textile by a rapier loom. **b** Photograph of the large-area sensing textile. **c** Photograph of the sensing unit in the textile. **d** Schematic diagram of the challenges that a sensor may encounter during space exploration. **e**, **f** Photograph of the sensing textile continuously transmitting signals in a frozen environment for 5 days. **g**, **h** Photograph of the sensing textile transmitting signals in boiled water and a vacuum chamber. **i** Photograph of the sensing textile being rolled by a car. **j** Schematic diagram of the circuit of the electronic glove and schematic diagram of cooperative work between electronic gloves and the textile display; ADC: analogue-to-digital converter; MCU: microcontroller unit. **k** Variations in the fiber strain sensor output voltage in the electronic glove for different gestures. Insets: photographs of astronauts' specific gestures triggering specific signals. Scale bars: 3 cm (**a**), 5 cm (**b**), 500 μm (**c**), 5 cm (**e**, **g**), 10 cm (**h**), 7 cm (**i**), and 8 cm (**k**)

textile (Fig. 4j, Fig. S9). Specifically, elastic gloves with predefined sensing units located at finger joints were prepared to show the gesture recognition capacity. Each sensing unit in the electronic glove can capture specific strain changes at predetermined finger joints, thus allowing the identification of overall gestures by integrating output voltage signals from multiple sensing units. The integrated signals were generated based on recognized gestures to drive a textile display system on the chest. As shown in Fig. 4k, different gestures elicited a distinct voltage response at various points on the electronic glove, triggering information such as oxygen levels and the distress signal "SOS".

4 Conclusions

In summary, we present a fiber strain sensor based on the mutual inductance effect. It exhibits outstanding linearity, cyclic stability, and durability. Due to the stability of its coaxial coiling structure, the sensor can withstand over 100,000 cycles and operate effectively under extreme conditions such as high/low temperature, compression, and torsion. Remarkably, the fiber strain sensor can be mass-produced and woven into textiles on a large scale, which holds significant potential in applications related to human–computer interactions.

Supplementary Information The online version contains supplementary material available at https://doi.org/10.1007/s42765-024-00445-1.

Acknowledgements YA and ZW contributed equally to this work. This work was financially by Ministry of Science and Technology of the People's Republic of China (2022YFA1203001, 2022YFA1203002), National Natural Science Foundation of China (T2321003, 22335003, T2222005, 22175042), and Science and Technology Commission of Shanghai Municipality (21511104900).

Author Contributions Yulu Ai: conceptualization, data curation, formal analysis, investigation, methodology, validation, visualization and writing. Zhen Wang: conceptualization, data curation, formal analysis, investigation, methodology, validation, visualization and writing. Yue Liu: data curation, formal analysis, investigation and methodology. Yuanyuan Zheng: validation and visualization. Jiaqi Wu: investigation and methodology. Junyi Zou: data curation and formal analysis. Songlin Zhang: validation and writing. Peining Chen: supervision, project administration and writing-review, editing and supporting. Huisheng Peng: supervision and project administration.

Data Availability The data that support the findings of this study are available from the corresponding author upon reasonable request.

Declarations

Conflict of interest Huisheng Peng is an editorial board member for *Advanced Fiber Materials* and was not involved in the editorial review or the decision to publish this article. All authors declare that there are no competing interests.

References

1. Shi X, Zuo Y, Zhai P, Shen JH, Yang YY, Gao Z, Liao M, Wu JX, Wang JW, Xu XJ, Tong Q, Zhang B, Wang BJ, Sun XM, Zhang LH, Pei QB, Jin DY, Chen PN, Peng HS. Large-area display textiles integrated with functional systems. *Nature*. **2021**;*591*:240–5.
2. Zhu ZF, Lin ZM, Zhai WJ, Kang XY, Song JT, Lu CH, Jiang HY, Chen PN, Sun XM, Wang BJ, Wang ZS, Peng HS. Indoor photovoltaic fiber with an efficiency of 25.53% under 1500 lux illumination. *Adv Mater*. **2024**;*36*:2304876.
3. He XY, Shi J, Hao YN, He MT, Cai JX, Qin XH, Wang LM, Yu JY. Highly stretchable, durable, and breathable thermoelectric fabrics for human body energy harvesting and sensing. *Carbon Energy*. **2022**;*4*:621–32.
4. Li M, Li Z, Qu L, Chen F, Tian M. Recent progress of the active materials with various micro-structures for flexible textile-based supercapacitors. *Adv Fiber Mater*. **2022**;*4*:1005–26.
5. He JQ, Lu CH, Jiang HB, Han F, Shi X, Wu JX, Wang LY, Chen TQ, Wang JJ, Zhang Y, Yang H, Zhang GQ, Sun XM, Wang BJ, Chen PN, Wang YG, Xia YY, Peng HS. Scalable production of high-performing woven lithium-ion fibre batteries. *Nature*. **2021**;*597*:57–63.
6. Liao M, Wang C, Hong Y, Zhang YF, Cheng XL, Sun H, Huang XL, Ye L, Wu JX, Shi X, Kang XY, Zhou XF, Wang JW, Li PZ, Sun XM, Chen PN, Wang BJ, Wang YG, Xia YY, Cheng YH, Peng HS. Industrial scale production of fibre batteries by a solution-extrusion method. *Nat Nanotechnol*. **2022**;*17*:372–7.
7. Li M, Li ZQ, Ye XR, He WZ, Qu LJ, Tian MW. A smart self-powered rope for water/fire rescue. *Adv Funct Mater*. **2023**;*33*:2210111.
8. Zhai WJ, Zhu ZF, Sun XM, Peng HS. Fiber solar cells from high performances towards real applications. *Adv Fiber Mater*. **2022**;*4*:1293–303.
9. Kang XY, Zhu ZF, Zhao TC, Zhai WJ, Xu JC, Lin ZM, Zeng KW, Wang BJ, Sun XM, Chen PN, Peng HS. Hierarchically assembled counter electrode for fiber solar cell showing record power conversion efficiency. *Adv Funct Mater*. **2022**;*32*:2207763.
10. Zhu ZF, Lin ZM, Gu Y, Song JT, Kang XY, Jiang HY, Peng HS. Designing reflective hybrid counter electrode for fiber dye-sensitized solar cell with record efficiency. *Adv Funct Mater*. **2023**;*33*:2306742.
11. Liu PY, Xiang Y, Liu Y, Peng SS, Zhu ZF, Shi X, Wu JX, Chen PN. Color-tunable light-emitting fibers for pattern displaying textiles. *J Mater Chem C*. **2024**;*3*:941.
12. Song JT, Gu Y, Lin ZM, Liu JZ, Kang XY, Gong XC, Liu PY, Yang YQ, Jiang HY, Wang JQ, Cao SW, Zhu ZF, Peng HS. Integrating light diffusion and conversion layers for highly efficient multicolored fiber-dye-sensitized solar cells. *Adv Mater*. **2024**;*36*:2312590.
13. Sundaram S, Kellnhofer P, Li Y, Zhu JY, Torralba A, Matusik W. Learning the signatures of the human grasp using a scalable tactile glove. *Nature*. **2019**;*569*:698–702.
14. Qaiser N, Al-Modaf F, Khan SM, Shaikh SF, El-Atab N, Hussain MM. A robust wearable point-of-care cnt-based strain sensor for wirelessly monitoring throat-related illnesses. *Adv Funct Mater*. **2021**;*31*:2103375.
15. He XY, Hao YN, He MT, Qin XH, Wang LM, Yu JY. Stretchable thermoelectric-based self-powered dual-parameter sensors with decoupled temperature and strain sensing. *ACS Appl Mater Interfaces*. **2021**;*13*:60498–507.
16. Ning C, Dong K, Cheng RW, Yi J, Ye CY, Peng X, Sheng FF, Jiang Y, Wang ZL. Flexible and stretchable fiber-shaped triboelectric nanogenerators for biomechanical monitoring and human-interactive sensing. *Adv Funct Mater*. **2021**;*31*:2006679.
17. Liu Y, Zhou XF, Yan H, Zhu ZF, Shi X, Peng YH, Chen L, Chen PN, Peng HS. Robust memristive fiber for woven textile memristor. *Adv Funct Mater*. **2022**;*32*:2201510.
18. Seyedin S, Uzun S, Levitt A, Anasori B, Dion G, Gogotsi Y, Razal JM. Mxene composite and coaxial fibers with high stretchability and conductivity for wearable strain sensing textiles. *Adv Funct Mater*. **2020**;*30*:1910504.
19. Ye XR, Shi BH, Li M, Fan Q, Qi XJ, Liu XH, Zhao SK, Jiang L, Zhang XJ, Fu K, Qu LJ, Tian MW. All-textile sensors for boxing punch force and velocity detection. *Nano Energy*. **2022**;*97*:107114.
20. Liu S, Ma K, Yang B, Li H, Tao XM. Textile electronics for VR/AR applications. *Adv Funct Mater*. **2021**;*31*:2007254.
21. Luo YY, Liu C, Lee YJ, Delpreto J, Wu K, Foshey M, Rus D, Palacios T, Li YZ, Torralba A, Matusik W. Adaptive tactile

interaction transfer via digitally embroidered smart gloves. *Nat Sci Rev*. **2024**;*15*:868.
22. Lama J, Yau A, Chen GR, Sivakumar A, Zhao X, Chen J. Textile triboelectric nanogenerators for self-powered biomonitoring. *J Mater Chem A*. **2021**;*9*:19149–78.
23. Xu Rd, She Mh, Jx L, Sk Z, Js Z, Zhang Xj Qu, Lj TM. Skin-friendly and wearable iontronic touch panel for virtual-real handwriting interaction. *ACS Nano*. **2023**;*17*:8293–302.
24. Seyedin S, Zhang P, Naebe M, Qin S, Chen J, Wang XG, Razal JM. Textile strain sensors: a review of the fabrication technologies, performance evaluation and applications. *Mater Horiz*. **2019**;*6*:219–49.
25. Chen CR, Feng JY, Li JX, Guo Y, Shi X, Peng HS. Functional fiber materials to smart fiber devices. *Chem Rev*. **2023**;*123*:613–62.
26. Liu ZK, Zhu TX, Wang JR, Zheng ZJ, Li Y, Li JS, Lai YK. Functionalized fiber-based strain sensors: Pathway to next-generation wearable electronics. *Nano-Micro Lett*. **2022**;*14*:61.
27. Liu ZY, Qi DP, Hu GY, Wang H, Jiang Y, Chen G, Luo YF, Loh XJ, Liedberg B, Chen XD. Surface strain redistribution on structured microfibers to enhance sensitivity of fiber-shaped stretchable strain sensors. *Adv Mater*. **2018**;*30*:1704229.
28. Guo Q, Pang WW, Xie X, Xu YL, Yuan WJ. Stretchable, conductive and porous mxene-based multilevel structured fibers for sensitive strain sensing and gas sensing. *J Mater Chem A*. **2022**;*10*:15634–46.
29. Zhao XX, Guo H, Ding P, Zhai W, Liu CT, Shen CY, Dai K. Hollow-porous fiber-shaped strain sensor with multiple wrinkle-crack microstructure for strain visualization and wind monitoring. *Nano Energy*. **2023**;*108*:108197.
30. Souri H, Banerjee H, Jusufi A, Radacsi N, Stokes AA, Park I, Sitti M, Amjadi M. Wearable and stretchable strain sensors: materials, sensing mechanisms, and applications. *Adv Intell Syst*. **2020**;*2*:2000039.
31. Sun HL, Bu YB, Liu H, Wang JW, Yang WK, Li QM, Guo ZH, Liu CT, Shen CY. Superhydrophobic conductive rubber band with synergistic dual conductive layer for wide-range sensitive strain sensor. *Sci Bull*. **2022**;*67*:1669–78.
32. Bu YB, Shen TY, Yang WK, Yang SY, Zhao Y, Liu H, Zheng YJ, Liu CT, Shen CY. Ultrasensitive strain sensor based on superhydrophobic microcracked conductive Ti_3C_2Tx mxene/paper for human-motion monitoring and e-skin. *Sci Bull*. **2021**;*66*:1849–57.
33. Wang CY, Guo HY, Wang P, Li JW, Sun YH, Zhang D. An advanced strategy to enhance teng output: Reducing triboelectric charge decay. *Adv Mater*. **2023**;*35*:2209895.
34. Sun JZ, Ren BQ, Han S, Shin H, Cha S, Lee J, Bae J, Park JJ. Amplified performance of charge accumulation and trapping induced by enhancing the dielectric constant via the cyano group of 3D-structured textile for a triboelectric multi-modal sensor. *Small Methods*. **2023**;*7*:2300344.
35. Yoon SG, Koo HJ, Chang ST. Highly stretchable and transparent microfluidic strain sensors for monitoring human body motions. *ACS Appl Mater Interfaces*. **2015**;*7*:27562–70.
36. Shen ZQ, Zhang ZL, Zhang NB, Li JH, Zhou PW, Hu FQ, Rong Y, Lu BY, Gu GY. High-stretchability, ultralow-hysteresis conductingpolymer hydrogel strain sensors for soft machines. *Adv Mater*. **2022**;*34*:2203650.
37. Choi DY, Kim MH, Oh YS, Jung SH, Jung JH, Sung HJ, Lee HW, Lee HM. Highly stretchable, hysteresis-free ionic liquid-based strain sensor for precise human motion monitoring. *ACS Appl Mater Interfaces*. **2017**;*9*:1770–80.
38. Zou J, Jing X, Chen Z, Wang SJ, Hu XS, Feng PY, Liu YJ. Multifunctional organohydrogel with ultralow-hysteresis, ultrafast-response, and whole-strain-range linearity for self-powered sensors. *Adv Funct Mater*. **2023**;*33*:2213895.
39. Li TQ, Li X, Yang JM, Sun HX, Sun JQ. Healable ionic conductors with extremely low-hysteresis and high mechanical strength enabled by hydrophobic domain-locked reversible interactions. *Adv Mater*. **2023**;*35*:2307990.
40. Yuan JF, Zhang YZ, Li GZ, Liu SQ, Zhu R. Printable and stretchable conductive elastomers for monitoring dynamic strain with high fidelity. *Adv Funct Mater*. **2022**;*32*:2204878.
41. Zhu T, Wu K, Wang Y, Zhang J, Liu G, Sun J. Highly stable and strain-insensitive metal film conductors via manipulating strain distribution. *Mater Horiz*. **2023**;*10*:5920–30.
42. Tian B, Fang YH, Liang J, Zheng K, Guo PW, Zhang XY, Wu Y, Liu Q, Huang ZD, Cao CY, Wu W. Fully printed stretchable and multifunctional e-textiles for aesthetic wearable electronic systems. *Small*. **2022**;*18*:2107298.
43. Sheng N, Ji P, Zhang MH, Wu ZT, Liang QQ, Chen SY, Wang HP. High sensitivity polyurethane-based fiber strain sensor with porous structure via incorporation of bacterial cellulose nanofibers. *Adv Electron Mater*. **2021**;*7*:2001235.
44. Li JY, Li S, Su YW. Stretchable strain sensors based on deterministic-contact-resistance braided structures with high performance and capability of continuous production. *Adv Funct Mater*. **2022**;*32*:2208216.
45. Chen S, Liu HZ, Liu SQ, Wang PP, Zeng SS, Sun LY, Liu L. Transparent and waterproof ionic liquid-based fibers for highly durable multifunctional sensors and strain-insensitive stretchable conductors. *ACS Appl Mater Interfaces*. **2018**;*10*:4305–14.
46. Bai YZ, Yin LT, Hou C, Zhou YL, Zhang F, Xu ZY, Li K, Huang YA. Response regulation for epidermal fabric strain sensors via mechanical strategy. *Adv Funct Mater*. **2023**;*33*:2214119.
47. Peng J, Wang B, Cheng HN, Yang RH, Yin YJ, Xu S, Wang CX. Highly sensitive and superhydrophobic fabric sensor based on agnps/polypyrrole composite conductive networks for body movement monitoring. *Compos Sci Technol*. **2022**;*227*:109561.
48. Wang S, Li S, Wang HM, Lu HJ, Zhu MJ, Wu XE, Liang HR, Liang XP, Zhang YY. Highly adhesive epidermal sensors with superior water-interference-resistance for aquatic applications. *Adv Funct Mater*. **2023**;*33*:2302687.
49. Park JI, Kim DK, Jang J, Kang IM, Kim H, Park J, Nam IW, Lang P, Bae JH. Control of silver nanowire-elastomer nanocomposite networks through elaborate direct printing for ultrathin and stretchable strain sensors. *Compos Sci Technol*. **2020**;*200*:108471.
50. Lu DX, Chu Y, Liao SQ, Li W, Cai YB, Wei QF, Wang QQ. Highly sensitive fabric strain sensor with double-layer conductive networks for joint rehabilitation therapy. *Compos Sci Technol*. **2022**;*230*:109778.
51. Chao MY, Wang YG, Ma D, Wu XX, Zhang WX, Zhang LQ, Wan PB. Wearable mxene nanocomposites-based strain sensor with tile-like stacked hierarchical microstructure for broad-range ultrasensitive sensing. *Nano Energy*. **2020**;*78*:105187.
52. Cai GM, Hao BW, Luo L, Deng ZM, Zhang RQ, Ran JH, Tang XN, Cheng DS, Bi SG, Wang X, Dai K. Highly stretchable sheath–core yarns for multifunctional wearable electronics. *ACS Appl Mater Interfaces*. **2020**;*12*:29717–27.
53. Wu L, Fan MS, Qu MJ, Yang ST, Nie J, Tang P, Pan LJ, Wang H, Bin YZ. Self-healing and anti-freezing graphene–hydrogel–graphene sandwich strain sensor with ultrahigh sensitivity. *J Mater Chem B*. **2021**;*9*:3088–96.
54. Huang T, He P, Wang RR, Yang SW, Sun J, Xie XM, Ding GQ. Porous fibers composed of polymer nanoball decorated graphene for wearable and highly sensitive strain sensors. *Adv Funct Mater*. **2019**;*29*:1903732.
55. Deng CH, Lan LF, He PH, Ding CC, Chen BZ, Zheng W, Zhao X, Chen WS, Zhong XZ, Li M, Tao H, Peng JB, Cao Y. High-performance capacitive strain sensors with highly stretchable vertical graphene electrodes. *J Mater Chem C*. **2020**;*8*:5541–6.
56. Park TH, Yu S, Cho SH, Kang HS, Kim Y, Kim MJ, Eoh H, Park C, Jeong B, Lee SW, Ryu DY, Huh J, Park C. Block copolymer structural color strain sensor. *NPG Asia Mater*. **2018**;*10*:328–39.

57. Cao PJ, Liu YW, Asghar W, Hu C, Li FL, Wu YZ, Li YY, Yu Z, Li SB, Shang J, Liu XC, Li RW. A stretchable capacitive strain sensor having adjustable elastic modulus capability for wide-range force detection. *Adv Energy Mater*. **2020**;*22*:1901239.
58. Jin H, Nayeem MOG, Lee S, Matsuhisa N, Inoue D, Yokota T, Hashizume D, Someya T. Highly durable nanofiber-reinforced elastic conductors for skin-tight electronic textiles. *ACS Nano*. **2019**;*13*:7905–12.
59. Zhou HW, Wang ZW, Zhao WF, Tong XM, Jin XL, Zhang XC, Yu Y, Liu HB, Ma YC, Li SS, Chen WX. Robust and sensitive pressure/strain sensors from solution processable composite hydrogels enhanced by hollow-structured conducting polymers. *Chem Eng J*. **2021**;*403*:126307.
60. Maddirala G, Searle T, Wang X, Alici G, Sencadas V. Multifunctional skin-compliant wearable sensors for monitoring human condition applications. *Appl Mater Today*. **2022**;*26*:101361.
61. Fu CY, Tang WY, Miao Y, Xu A, Nilghaz A, Xu WL, Dong K, Su B, Xia ZG. Large-scalable fabrication of liquid metal-based double helix core-spun yarns for capacitive sensing, energy harvesting, and thermal management. *Nano Energy*. **2023**;*106*:108078.
62. Lee J, Ihle SJ, Pellegrino GS, Kim H, Yea J, Jeon CY, Son HC, Jin C, Eberli D, Schmid F, Zambrano BL, Renz AF, Forró C, Choi H, Jang KI, Küng R, Vörös J. Stretchable and suturable fibre sensors for wireless monitoring of connective tissue strain. *Nat Electron*. **2021**;*4*:291–301.
63. Kim SR, Kim JH, Park JW. Wearable and transparent capacitive strain sensor with high sensitivity based on patterned ag nanowire networks. *ACS Appl Mater Interfaces*. **2017**;*9*:26407–16.
64. Xu F, Zhu Y. Highly conductive and stretchable silver nanowire conductors. *Adv Mater*. **2012**;*24*:5117–22.
65. Zhang WX, Miao JL, Zuo XW, Zhang XJ, Qu LJ. Weaving a magnificent world: 1D fibrous electrodes and devices for stretchable and wearable electronics. *J Mater Chem C*. **2022**;*10*:14027–52.
66. Chen JL, He TY, Du ZQ, Lee CK. Review of textile-based wearable electronics: from the structure of the multi-level hierarchy textiles. *Nano Energy*. **2023**;*117*:108898.

Publisher's Note Springer Nature remains neutral with regard to jurisdictional claims in published maps and institutional affiliations.

Springer Nature or its licensor (e.g. a society or other partner) holds exclusive rights to this article under a publishing agreement with the author(s) or other rightsholder(s); author self-archiving of the accepted manuscript version of this article is solely governed by the terms of such publishing agreement and applicable law.